$\kappa_s$, all coherences will ultimately disappear. However, for large enough $\kappa_2$, a quantum superposition transient state is observed.

In this experiment, we achieve $|\xi_p|^2 = 1.2$, which implies $g_2/2\pi$ = 111 kHz and $\kappa_2/\kappa_s$ = 1.0. The quantum nature of the transient storage state is visible in the negative fringes of the Wigner function (see Fig. 4, A and B; 7 μs) and the non-Poissonian photon number statistics (Fig. 4D; 7 μs). After 7 μs of pumping, we obtain a state with an average photon number $\overline{n} = 2.4$ and a parity of 42%, which is larger than the parity of a thermal state (17%) or a coherent state (0.8%) with equal $\overline{n}$. After 19 μs of pumping, although the negative fringes vanish, the phase and amplitude of the SSSs $|\pm\alpha_\infty\rangle$ are conserved. Our data are in good agreement with numerical simulations (Fig. 4C), indicating that our dominant source of imperfection is single-photon loss. These results illustrate the confinement of the storage state into the manifold of SSSs and how it transits through a quantum superposition of $|\pm\alpha_\infty\rangle$.

We have realized a nonlinearly driven dissipative oscillator that spontaneously evolves toward the quantum manifold spanned by two coherent states. This was achieved by attaining the regime in which the photon-pair exchange rate is of the same order as the single-photon decay rate. The ratio between these two rates can be further improved within the present technology by using an oscillator with a higher quality factor and increasing the oscillator's nonlinear coupling to the bath. Our experiment is an essential step toward a new paradigm for universal quantum computation (*11*). By combining higher-order forms of our nonlinear dissipation with efficient error syndrome measurements (*28*), quantum information can be encoded and manipulated in a protected manifold of quantum states.

## REFERENCES AND NOTES


1. C. Sayrin *et al.*, *Nature* **477**, 73–77 (2011).
2. R. Vijay *et al.*, *Nature* **490**, 77–80 (2012).
3. D. Ristè, C. C. Bultink, K. W. Lehnert, L. DiCarlo, *Phys. Rev. Lett.* **109**, 240502 (2012).
4. P. Campagne-Ibarcq *et al.*, *Phys. Rev. X* **3**, 021008 (2013).
5. H. Krauter *et al.*, *Phys. Rev. Lett.* **107**, 080503 (2011).
6. K. W. Murch *et al.*, *Phys. Rev. Lett.* **109**, 183602 (2012).
7. S. Shankar *et al.*, *Nature* **504**, 419–422 (2013).
8. Y. Lin *et al.*, *Nature* **504**, 415–418 (2013).
9. M. Wolinsky, H. J. Carmichael, *Phys. Rev. Lett.* **60**, 1836–1839 (1988).
10. A. Wallraff *et al.*, *Nature* **431**, 162–167 (2004).
11. M. Mirrahimi *et al.*, *New J. Phys.* **16**, 045014 (2014).
12. G. Kirchmair *et al.*, *Nature* **495**, 205–209 (2013).
13. J. D. Teufel *et al.*, *Nature* **475**, 359–363 (2011).
14. P. Drummond, Z. Ficek, Eds., *Quantum Squeezing* (Series on Atomic, Optical, and Plasma Physics, Springer, Berlin, 2004).
15. I. Siddiqi *et al.*, *Phys. Rev. Lett.* **93**, 207002 (2004).
16. M. A. Castellanos-Beltran, K. D. Irwin, G. C. Hilton, L. R. Vale, K. W. Lehnert, *Nat. Phys.* **4**, 929–931 (2008).
17. See the supplementary materials on *Science* Online for details.
18. H. J. Carmichael, *Statistical Methods in Quantum Optics 2* (Series on Theoretical and Mathematical Physics, Springer, Berlin, 2008).
19. B. Johnson *et al.*, *Nat. Phys.* **6**, 663–667 (2010).
20. M. I. Dykman, M. A. Krivoglaz, *Physica A* **104**, 480–494 (1980).
21. A. Ourjoumtsev, H. Jeong, R. Tualle-Brouri, P. Grangier, *Nature* **448**, 784–786 (2007).
22. B. Vlastakis *et al.*, *Science* **342**, 607–610 (2013).
23. S. Deléglise *et al.*, *Nature* **455**, 510–514 (2008).
24. C. Monroe, D. M. Meekhof, B. E. King, D. J. Wineland, *Science* **272**, 1131–1136 (1996).
25. M. Hofheinz *et al.*, *Nature* **459**, 546–549 (2009).
26. L. G. Lutterbach, L. Davidovich, *Phys. Rev. Lett.* **78**, 2547–2550 (1997).
27. S. Haroche, J.-M. Raimond, *Exploring the Quantum: Atoms, Cavities and Photons* (Oxford Univ. Press, Oxford, 2006).
28. L. Sun *et al.*, *Nature* **511**, 444–448 (2014).
29. D. I. Schuster *et al.*, *Nature* **445**, 515–518 (2007).


## ACKNOWLEDGMENTS


We thank L. Jiang and V. V. Albert for helpful discussions. Facilities use was supported by the Yale Institute for Nanoscience and Quantum Engineering and NSF Materials Research Science and Engineering Center Division of Material Research award 1119826. This research was supported by the Army Research Office under grant W911NF-14-1-0011. M.M. acknowledges support from the French Agence Nationale de la Recherche under the project EPOQ2 number ANR-09-JCJC-0070. S.T. acknowledges support from ENS Cachan.


## SUPPLEMENTARY MATERIALS

www.sciencemag.org/content/347/6224/853/suppl/DC1
Materials and Methods
Supplementary Text
Figs. S1 to S11
Tables S1 and S2
References (*30*–*37*)


31 October 2014; accepted 22 January 2015
10.1126/science.aaa2085


OPTICS

# Spatially structured photons that travel in free space slower than the speed of light


**Daniel Giovannini,[1]* Jacquiline Romero,[1]* Václav Potoček,[1,2] Gergely Ferenczi,[1] Fiona Speirits,[1] Stephen M. Barnett,[1] Daniele Faccio,[3] Miles J. Padgett[1]†**



**That the speed of light in free space is constant is a cornerstone of modern physics. However, light beams have finite transverse size, which leads to a modification of their wave vectors resulting in a change to their phase and group velocities. We study the group velocity of single photons by measuring a change in their arrival time that results from changing the beam's transverse spatial structure. Using time-correlated photon pairs, we show a reduction in the group velocity of photons in both a Bessel beam and photons in a focused Gaussian beam. In both cases, the delay is several micrometers over a propagation distance of ~1 meter. Our work highlights that, even in free space, the invariance of the speed of light only applies to plane waves.**


The speed of light is trivially given as $c/n$, where $c$ is the speed of light in free space and $n$ is the refractive index of the medium. In free space, where $n$ = 1, the speed of light is simply $c$. We show that the introduction of transverse structure to the light beam reduces the group velocity by an amount that depends on the aperture of the optical system. The delay corresponding to this reduction in the group velocity can be greater than the optical wavelength and consequently should not be confused with the ≈π Gouy phase shift (*1*, *2*). To emphasize that this effect is both a linear and intrinsic property of light, we measure the delay as a function of the transverse spatial structure of single photons.

The slowing down of light that we observe in free space should also not be confused with slow, or indeed fast, light associated with propagation in highly nonlinear or structured materials (*3*, *4*). Even in the absence of a medium, the modification of the speed of light has previously been known. For example, within a hollow waveguide, the wave vector along the guide is reduced below the free-space value, leading to a phase velocity $v_\phi$ greater than $c$. Within the hollow waveguide, the product of the phase and group velocities is given as $v_\phi v_{g,z} = c^2$, thereby resulting in a group velocity $v_{g,z}$ along the waveguide less than $c$ (*5*).

Although this relation for group and phase velocities is derived for the case of a hollow waveguide, the waveguide material properties are irrelevant. It is the transverse spatial confinement of the field that leads to a modification of the axial component of the wave vector, $k_z$. In general, for light of wavelength λ, the magnitude of the wave vector, $k_0 = 2\pi/\lambda$, and its Cartesian components $\{k_x, k_y, k_z\}$ are related through (*5*)

$$k_z^2 + k_x^2 + k_y^2 = k_0^2$$

All optical modes of finite $x,y$ spatial extent require nonzero $k_x$ and $k_y$, which implies $k_z < k_0$, giving a corresponding modification of both the phase and group velocities of the light. In this sense, light beams with nonzero $k_x$ and $k_y$ are naturally dispersive, even in free space.

Extending upon the case of a mode within a hollow waveguide, an example of a structured


[1]School of Physics and Astronomy, Scottish Universities Physics Alliance (SUPA), University of Glasgow, Glasgow G12 8QQ, UK. [2]Faculty of Nuclear Sciences and Physical Engineering, Czech Technical University in Prague, Břehová 7, 115 19 Praha 1, Czech Republic. [3]School of Engineering and Physical Sciences, SUPA, Heriot-Watt University, Edinburgh EH14 4AS, UK.
*These authors contributed equally to this work. †Corresponding author. E-mail: miles.padgett@glasgow.ac.uk

beam is a Bessel beam (Fig. 1A), which is itself the description of a mode within a circular waveguide (*1*, *6*). In free space, Bessel beams can be created with an axicon, or its diffractive optical equivalent (*7*), that converts a plane wave into conical phase fronts characterized by a single radial component of the wave vector, $k_r = \sqrt{k_x^2 + k_y^2}$ (*8*–*10*). This single value of the radial component gives a unique value of $k_z < k_0$ and hence uniquely defined phase and group velocities (*11*).

To avoid complications arising from the finite thickness of refractive optical elements, we use diffractive optics, idealized as having zero thickness. For a Bessel beam created with a diffractive optic (*7*), characterized by $k_r$ (with $k_r << k_0$), the axial component of the wave vector is given by $k_z = k_0 - k_r^2/2k_0$. The resulting phase velocity and group velocity along $z$ are

$$v_\phi = c\left(1 - \frac{k_r^2}{2k_0^2}\right)^{-1}$$

and

$$v_{g,z} = c\left(1 - \frac{k_r^2}{2k_0^2}\right)$$

This modification of the phase and group velocities of Bessel beams has been examined in the classical, many-photon regime. Subtle changes in velocity have been previously studied with Bessel beams in the microwave (*12*) and optical regimes (*13*–*15*).

We demonstrate the intrinsic and linear nature of this reduction in group velocity by measuring the delay in the arrival time of single photons. Over a propagation distance of $L$, the reduction in the group velocity compared to the plane-wave case gives a delay of

$$\delta z_{\text{Bessel}} \approx L\frac{k_r^2}{2k_0^2} = \frac{L}{2}\alpha^2 \qquad (1)$$

As an example, for an axicon designed to produce $\alpha = k_r/k_0 = 4.5 \times 10^{-3}$ over a propagation distance of 1 m, we predict a delay of ~30 fs, corresponding to a spatial delay of 10 μm.

To measure the arrival time of single photons with femtosecond precision, we adopt a method relying upon a quantum effect, namely, the Hong-Ou-Mandel (HOM) interference (*16*). A parametric down-conversion source is used to produce photon pairs that are strongly correlated in their wavelengths and their generation time. One photon can then act as a reference, against which the arrival of the other photon can be compared (Fig. 2). This second photon goes through a free-space propagation section, in which a first spatial light modulator (SLM) can be programmed to act as a diffractive optical element implementing axicons or lenses. A second SLM then reverses the structuring introduced by the first. When the arrival times of the two photons incident on a beam splitter are matched to a precision better than their coherence time, both photons emerge from the same output port. Under this matched condition, the coincidence rate for detection at the two output ports of the beam splitter falls to zero, which results in what is known as a HOM dip. The position of the dip is recorded as a function of the spatial shaping of the photon propagating in free space.

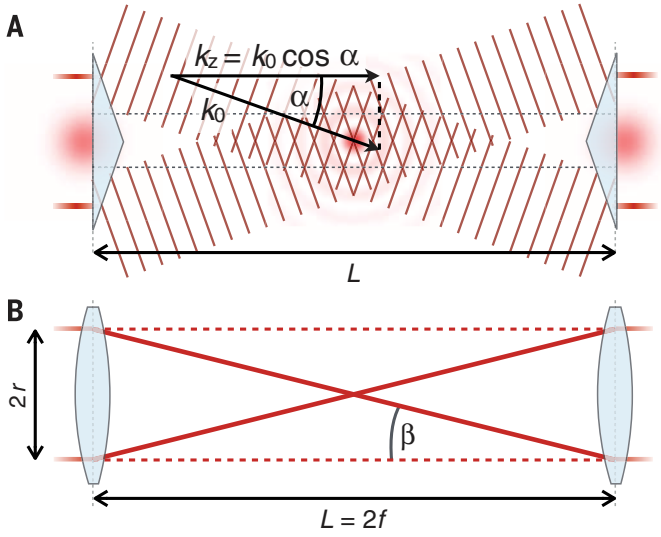


**Fig. 1. Adding spatial structure to a light beam.** (**A**) A Bessel beam can be created with an axicon, producing conical phase fronts of angle α. (**B**) A ray entering a confocal telescope at radius $r$ will travel an additional distance proportional to $\cos^{-1}\beta$.

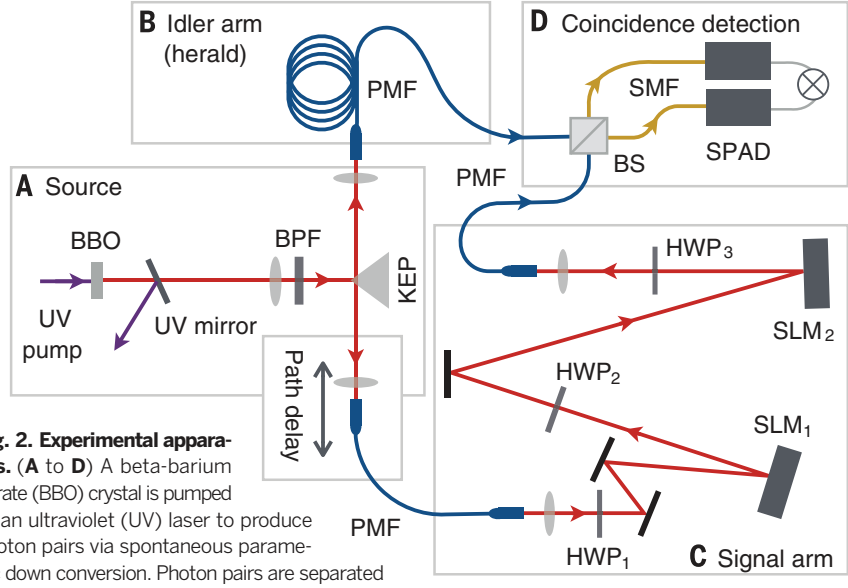


**Fig. 2. Experimental apparatus.** (**A** to **D**) A beta-barium borate (BBO) crystal is pumped by an ultraviolet (UV) laser to produce photon pairs via spontaneous parametric down conversion. Photon pairs are separated by a knife edge prism (KEP); a band-pass filter (BPF) sets the spectral profile of the down-converted light. Half-wave plates (HWP) are used to maximize the efficiency of the spatial light modulators (SLM) and match the polarization of the polarization-maintaining fibers (PMF). Signal and idler photons enter a fiber-coupled beam splitter (BS) (*21*), whose outputs are single-mode fibers (SMF) connected to avalanche photodiodes (SPAD). The SPADs feed a coincidence counter.

Taking the Bessel beam as our first example, the transverse structuring can be turned on and off for each value of path delay. The corresponding position of the HOM dip can then be directly compared between the two cases. Figure 3A shows the baseline-normalized coincidences for two different values of $\alpha = k_r/k_0$ (where we define the baseline as the coincidence count at path delay far from the dip position). In all cases, the width of the HOM dips is the same, set by the 10-nm spectral bandwidth of the down-converted photons. The key result is that the HOM dip associated with the Bessel beam is delayed with respect to the dip obtained for a collimated beam. We measure a delay of 2.7 ± 0.8 μm for the case of $\alpha_1 = 0.00225$ rad and 7.7 ± 0.8 μm for $\alpha_2 = 0.00450$ rad. These measured values agree with theoretical predictions of 2.0 and 8.1 μm for $\alpha_1$ and $\alpha_2$, respectively.

The analytical form of this predicted delay (Eq. 1) suggests a simple geometrical model, where the delay arises from the additional length of the diagonal ray, propagating at an angle α with respect to the optical axis. In Fig. 3B, we compare the measured and predicted values for the delay, showing that Eq. 1 is valid over the range of angles that we tested for the Bessel beam.

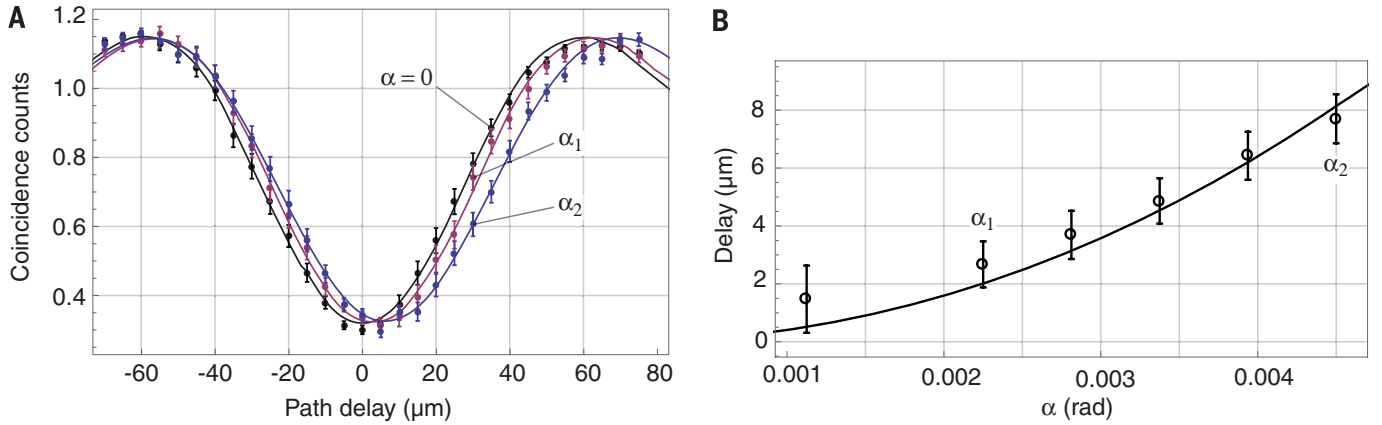


**Fig. 3. Experimental results for a Bessel beam.** (**A**) Measured HOM dips for two values of α ($\alpha_1$ = 0.00225, red; $\alpha_2$ = 0.00450, blue) and the α = 0 case (black), with corresponding best fits (*16*). (**B**) Measured delays (open circles) and theoretical prediction from Eq. 1 (solid line), for different values of α. The delays are expressed with respect to the α = 0 case. corresponding to an unstructured collimated beam.

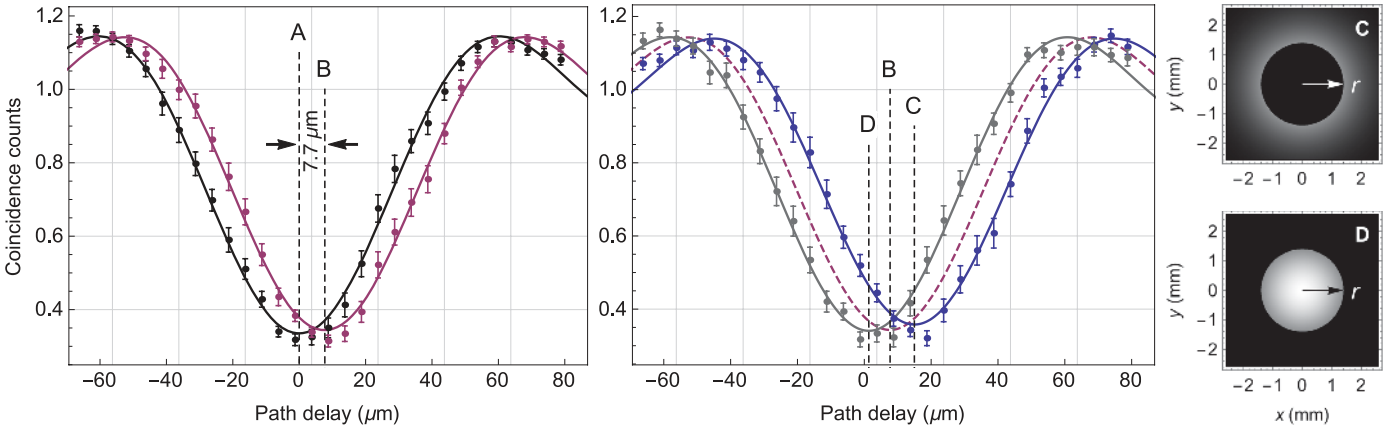


**Fig. 4. Measured HOM dips for collimated and focused Gaussian beams.** (**Left**) HOM dip comparison for collimated (black) and focused (red) Gaussian beam. Minima are marked by A and B. (**Right**) HOM dip comparison for cases with an $r$ = 1.4 mm center stop (blue, corresponding to inset C), and an edge stop of the same radius (gray, corresponding to inset D). Minima are marked by C and D. The red dashed curve is shown as a reference.

Perhaps the most common form of spatial structuring of a light beam is focusing, which also leads to a modification of the axial component of the wave vector. We consider the propagation of light through a telescope comprising two identical lenses separated by twice their focal length, $f$ (i.e., a confocal telescope). Assuming a ray-optical model, a coaxial ray incident upon the first lens at radius $r$ emerges from the second lens coaxially at the same radius but inverted about the optical axis (Fig. 1B). Comparing the on-axis separation of the lenses to this diagonal distance gives an additional distance traveled of $\delta z = L/\cos\beta - L \approx r^2/f$, where β is the angle between ray and optical axis.

For a beam of Gaussian intensity distribution with $1/e^2$ radius $w$, the expectation value of $r^2$ is $\langle r^2 \rangle = w^2/2$. Therefore, the expected delay $\delta z_{\text{Gauss}}$ for a Gaussian beam on transmission through a confocal telescope is

$$\delta z_{\text{Gauss}} = w^2/2f = (w/f)^2 \times f/2 \qquad (2)$$

where $w$ is the waist of the input beam. The delay is a quadratic function of the quantity $w/f$, which can be considered as a measure of the beam divergence, defined by the numerical aperture of the system. The delay increases with increasing numerical aperture. This geometrical model and a rigorous theoretical calculation provide the same results for both the Bessel and confocal cases, within the same approximations (*17*, *18*). The full theoretical model, however, applies to any arbitrary field. As the delay increases with the square of the numerical aperture, the delay becomes progressively harder to detect at longer distances.

The delay arising from focusing is shown in Fig. 4. Trace A shows the position of the HOM dip for the case of a collimated beam, and trace B shows its position for the case of $f$ = 0.40 m. We measure a delay of 7.7 ± 0.4 μm for the focused case. This is comparable to the predicted delay based on Eq. 2 which, for our beam of $w$ = 2.32 ± 0.09 mm, is 6.7 ± 0.6 μm. The slight difference between our measurement and the predicted value is likely due to residual aberrations and imperfect collimation, leading to an ill-defined beam waist, upon which the delay is quadratically dependent.

We further investigate the dependence of the delay upon the beam structure by introducing aperture restrictions to the beam, in the form of center and edge stops (Fig. 4, insets). Results are shown in traces C and D in Fig. 4, together with the full-aperture focused beam case (red line, trace B). A center stop increases the expectation value of $r^2$, thereby increasing the delay compared to the full-aperture case. Trace C shows the dip with a center stop of radius 1.4 mm, as shown in inset C. We measure a dip position additionally delayed by 7.3 ± 0.4 μm compared to the full-aperture focused beam, giving a total delay of 15.0 ± 0.6 μm. Next, we introduce an edge stop of the same radius, as shown in inset D. By restricting the aperture, the expectation value of $r^2$ is decreased, decreasing the delay with respect to the collimated case. Trace D shows the position of the HOM dip, which is now reduced by 6.4 ± 0.4 μm with respect to the full-aperture case, resulting in a total delay compared to the collimated case of 1.3 ± 0.6 μm.

It is important to consider three possible sources of systematic errors. First, the phase values of all the pixels of the SLMs lie between 0 and 2π with an average value of ≈π. Regardless of what optical component is encoded on the SLMs, the effective thickness of the liquid crystal, as averaged over the full aperture, remains the same.

Consequently, the observed delay is not a result of the SLMs themselves. Second, the width of the HOM dip remains compatible with the interference filter used. Therefore, the coherence time of the light is unchanged by the setting of the SLMs and hence the magnitude of the delays cannot be a result of spectral postselection. Third, one must ensure that the delays are not due to misalignment in the optical paths. In aligning the experiment, we used back-projection (*19*). More important, the alignment for the cases that have aperture restrictions remains the same (the coaxial apertures do not change the path of the beam). Hence, the delays that we measure can only result from the transverse structure of the beam and indeed are consistent with our theoretical predictions.

Our measurement of group velocity is strictly a measurement of the difference in propagation speed between a reference photon and a spatially structured photon. No direct measurement of the speed of light is made. Within this manuscript, the velocity that we measure is strictly the group velocity of the photons (*20*).

The speed of light in free-space propagation is a fundamental quantity. It holds a pivotal role in the foundations of relativity and field theory, as well as in technological applications such as time-of-flight measurements. It has previously been experimentally established that single photons travel at the group velocity (*20*). We have now shown that transverse structuring of the photon results in a decrease in the group velocity along the axis of propagation. We emphasize that in our full-aperture experiments, no pre- or post-selection is applied to the spatially structured photons and that the group velocities are always compared over the same propagation distance, much as if they were in a race. The effect can be derived from a simple geometric argument, which is also supported by a rigorous calculation of the harmonic average of the group velocity. Beyond light, the effect observed will have applications to any wave theory, including sound waves.

## REFERENCES AND NOTES


1. A. Yariv, *Quantum Electronics* (Wiley, New York, ed. 3, 1989).
2. S. Feng, H. G. Winful, *Opt. Lett.* **26**, 485–487 (2001).
3. R. W. Boyd, D. J. Gauthier, *Science* **326**, 1074–1077 (2009).
4. J. E. Vornehm Jr., R. W. Boyd, in *Tutorials in Complex Photonic Media*, M. A. Noginov, G. Dewar, M. W. McCall, N. I. Zheludev, Eds. (SPIE, Bellingham, WA, 2009), chap. 19.
5. I. S. Grant, W. R. Phillips, *Electromagnetism* (Wiley, New York, 1980).
6. E. R. Nagelberg, J. Shefer, *Bell Syst. Tech. J.* **44**, 1321–1338 (1965).
7. S. Klewitz, S. Sogomonian, M. Woerner, S. Herminghaus, *Opt. Commun.* **154**, 186–190 (1998).
8. R. M. Herman, T. A. Wiggins, *J. Opt. Soc. Am. A* **8**, 932–942 (1991).
9. J. H. McLeod, *J. Opt. Soc. Am.* **44**, 592 (1954).
10. A. Vasara, J. Turunen, A. T. Friberg, *J. Opt. Soc. Am. A* **6**, 1748–1754 (1989).
11. J. T. Lunardi, *Phys. Lett. A* **291**, 66–72 (2001).
12. D. Mugnai, A. Ranfagni, R. Ruggeri, *Phys. Rev. Lett.* **84**, 4830–4833 (2000).
13. K. B. Kuntz *et al.*, *Phys. Rev. A* **79**, 043802 (2009).
14. I. Alexeev, K. Y. Kim, H. M. Milchberg, *Phys. Rev. Lett.* **88**, 073901 (2002).
15. P. W. Milonni, *J. Phys. B* **35**, R31–R56 (2002).
16. C. K. Hong, Z. Y. Ou, L. Mandel, *Phys. Rev. Lett.* **59**, 2044–2046 (1987).
17. Z. L. Horváth, J. Vinko, Zs. Bor, D. von der Linde, *Appl. Phys. B* **63**, 481–484 (1996).
18. Materials and methods are available as supplementary materials on *Science* Online.
19. M. McLaren, J. Romero, M. J. Padgett, F. Roux, A. Forbes, *Phys. Rev. A* **88**, 033818 (2013).
20. A. M. Steinberg, P. G. Kwiat, R. Y. Chiao, *Phys. Rev. Lett.* **68**, 2421–2424 (1992).
21. R. Kaltenbaek, B. Blauensteiner, M. Żukowski, M. Aspelmeyer, A. Zeilinger, *Phys. Rev. Lett.* **96**, 240502 (2006).


## ACKNOWLEDGMENTS

We thank S. Franke-Arnold for useful discussions. This work was supported by the Engineering and Physical Sciences Research Council through the COAM program, and by the European Research Council (ERC) through the TWISTS grant; D.F. acknowledges support from ERC through the MOLIGHT project. We thank Hamamatsu for their support. M.J.P. thanks the Royal Society.

M.J.P., D.F. and S.M.B. conceived the experiment and supervised the work; M.J.P., D.G., and J.R. designed the experiment; D.G. and J.R. constructed the experiment, acquired the data, and carried out the data analysis; V.P., J.R., G.F., F.S., and S.M.B. further developed the theoretical model; J.R., D.G., and M.J.P. wrote the text with input from all coauthors.

## SUPPLEMENTARY MATERIALS

www.sciencemag.org/content/347/6224/857/suppl/DC1
Materials and Methods
Supplementary Text

14 November 2014; accepted 8 January 2015
Published online 22 January 2015;
10.1126/science.aaa3035

GALAXY EVOLUTION

# Black hole feedback in the luminous quasar PDS 456

**E. Nardini,[1]* J. N. Reeves,[1,2] J. Gofford,[1,2] F. A. Harrison,[3] G. Risaliti,[4,5] V. Braito,[6] M. T. Costa,[1] G. A. Matzeu,[1] D. J. Walton,[3,7] E. Behar,[8] S. E. Boggs,[9] F. E. Christensen,[10] W. W. Craig,[11] C. J. Hailey,[12] G. Matt,[13] J. M. Miller,[14] P. T. O'Brien,[15] D. Stern,[7] T. J. Turner,[16,17] M. J. Ward[18]**

**The evolution of galaxies is connected to the growth of supermassive black holes in their centers. During the quasar phase, a huge luminosity is released as matter falls onto the black hole, and radiation-driven winds can transfer most of this energy back to the host galaxy. Over five different epochs, we detected the signatures of a nearly spherical stream of highly ionized gas in the broadband x-ray spectra of the luminous quasar PDS 456. This persistent wind is expelled at relativistic speeds from the inner accretion disk, and its wide aperture suggests an effective coupling with the ambient gas. The outflow's kinetic power larger than $10^{46}$ ergs per second is enough to provide the feedback required by models of black hole and host galaxy coevolution.**

Disk winds are theoretically expected as a natural consequence of highly efficient accretion onto supermassive black holes (*1*), as the energy radiated in this process might easily exceed the local binding energy of the gas. In the past few years, black hole winds with column densities of ~$10^{23}$ cm$^{-2}$ and velocities of ~0.1 times the speed of light ($c$) have been revealed in a growing number of nearby active galactic nuclei (AGN) through blueshifted x-ray absorption lines (*2*, *3*). Outflows of this kind are commonly believed to affect the dynamical and physical properties of the gas in the host galaxy, and, hence, its star formation history (*4*). However, a complete observational characterization of how this feedback works is still missing. On its own, the detection of narrow, blueshifted features does not convey any information about the opening angle or the ejection site of the wind. This knowledge is critical for measuring the total power carried by the outflow, whose actual influence on galactic scales remains unclear (*5*).

The nearby ($z$ = 0.184) radio-quiet quasar PDS 456 is an established Rosetta stone for studying disk winds (*6*–*8*). With a bolometric luminosity $L_{bol}$ ~ $10^{47}$ erg/s and a mass of the central black hole on the order of $10^9$ solar masses ($M_{Sun}$) (*9*), it is an exceptionally luminous AGN in the local universe and might be regarded as a counterpart of the accreting supermassive black holes during the peak of quasar activity at high redshift. Since the earliest x-ray observations, PDS 456 has regularly exhibited a deep absorption trough at rest-frame energies above 7 keV (*6*), which was occasionally resolved with high statistical significance into a pair of absorption lines at ~9.09 and 9.64 keV (*7*). Because no strong atomic transitions from cosmically abundant elements correspond to these energies, such lines are most likely associated with resonant K-shell absorption from Fe XXV He$\alpha$ (6.7 keV) and Fe XXVI Ly$\alpha$ (6.97 keV) in a wind with an outflow velocity of ~0.3 $c$.

The X-ray Multi-Mirror Mission (XMM)–Newton and Nuclear Spectroscopic Telescope Array (NuSTAR) satellites simultaneously observed PDS 456 on four occasions in 2013, between 27 August and 21 September. A fifth observation was performed several months later, on 26 February 2014 (table S1). The entire campaign caught the quasar in widely different spectral states (Fig. 1). The broad Fe-K absorption trough is conspicuous at all times against a simple baseline continuum, with an equivalent width